## PAPER

# Studies of adsorption of α,β-unsaturated carbonyl compounds on heterogeneous Au/CeO$_2$, Au/TiO$_2$ and Au/SiO$_2$ catalysts during reduction by hydrogen†

Maciej Zielinski, [ID] *[ab] Wojciech Juszczyk [ID] [a] and Zbigniew Kaszkur [ID] [a]

Our research focuses on phenomena accompanying adsorption of mesityl oxide (4-methylpent-3-en-2-one) on the surface of heterogeneous supported gold catalysts: Au/CeO$_2$, Au/TiO$_2$ and Au/SiO$_2$. We have studied reduction in the gas phase of (volatile) α,β-unsaturated carbonyl compounds (R-(V)ABUCC) which mesityl oxide is a basic model of. *In situ* infrared (IR) spectroscopy was employed to establish that the most active catalysts allow adsorption of conjugated ketones or aldehydes in the enolate (*i.e.* bridge-like adsorption through the oxygen from the carbonyl group and the β-carbon) and carboxylic form or with the $^\alpha$C$=^\beta$C double bond on a Lewis acidic site. Reductive properties of the catalysts and pure supports were studied by temperature-programmed reduction (TPR). We show that cerium(IV) oxide (CeO$_2$, ceria) and titanium(IV) oxide (TiO$_2$, titania) when decorated with gold nanoparticles (AuNP) can interact with hydrogen at temperatures approx. 150 °C lower than typical for pure oxides what includes even cyclic adsorption and instant release of H$_2$ below 100 °C in the case of gold–ceria system. Morphology and structure characterisation by transmission electron microscopy (TEM) and powder X-ray diffraction (PXRD) confirms that, with the obtained Au loadings, we achieved excellent dispersion of AuNPs while maintaining their small size, preferably below 5 nm, even though the Au/CeO$_2$ catalyst contained broad distribution of AuNPs sizes.

## Introduction

The development of the technology of the next generation of catalysts, especially the promising gold (Au) catalysts, and their prospective application in industrial processes depend now on the knowledge explaining why the desired properties occur. This research focuses on heterogeneous nanocrystalline Au (AuNCr) catalysts based on oxide supports: silica (SiO$_2$), ceria (cerium(IV) oxide, CeO$_2$) and titanium(IV) oxide (TiO$_2$). These systems exhibit different chemical properties in reduction of (volatile) α,β-unsaturated carbonyl compounds (R-(V)ABUCC) with gaseous hydrogen. We believe that mutual influence of support on gold and *vice versa* provides occurrence of desired properties (such phenomenon is referred to as metal–support interaction, MSI[1–3]). Utilisation of gold-based systems (*e.g.* ref. 4) creates additional solution, with regard to existing ones (*e.g.* ref. 5–10), to precisely control the hydrogenation pathway and, thus, to obtain desired products. The main scope of this work is to describe surface adsorption phenomena by *in situ* infrared (IR) spectroscopy that can later be utilised for studies of catalyst surface structure changes by means of various structure-sensitive techniques arranged as *in operando* setups, including *in operando* electron microscopy,[11] *in operando* powder X-ray diffraction[12,13] and others *e.g.* ref. 14.

Hydrogenation of conjugated unsaturated carbonyl compounds (*i.e.* aldehydes and ketones) is the process of great importance in which valuable commodities are obtained, to mention just printer inks,[15] perfumes[5,16] and medicines.[17] In the first step (Fig. 1), unsaturated alcohol (so called allylic alcohol) or saturated carbonyl compound are produced. Next step leads always to the same product: saturated alcohol. Allylic alcohols production is of special interest of manufacturers, as currently these compounds are synthesised in costly stoichiometric reactions with NaBH$_4$, Grignard compounds or homogeneous catalysts containing heavy metals that can assure *e.g.* high enantiomeric purity.[17] Although gold catalysts exhibit desired properties, exhaustive answers covering ensuring long-time stability of catalysts and key physicochemical features responsible for observed phenomena are still not fully provided.

Reaction in the gas phase, as chosen for this project, has numerous advantages. Lack of solvent eliminates the necessity of taking it into account in preparation of the *in situ* experiment

$^a$Institute of Physical Chemistry, Polish Academy of Sciences, ul. M. Kasprzaka 44/52, 01-224 Warszawa, Poland. E-mail: mzielinski@ichf.edu.pl

$^b$National Centre for Nuclear Research, NOMATEN Centre of Excellence, ul. A. Soltana 7, 05-400 Otwock-Swierk, Poland
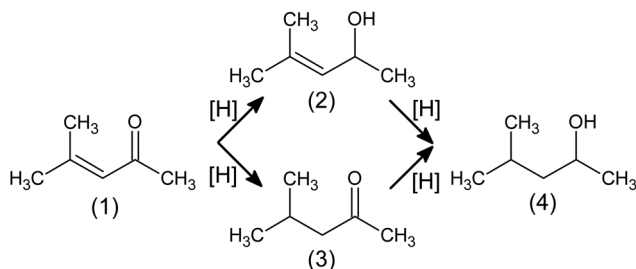
**Fig. 1** Hydrogenation pathways of mesityl oxide (4-methylpent-3-en-2-one, (**1**)) to its derivatives: 4-methylpent-3-en-2-ol (**2**); 4-methyl-pentan-2-one (**3**); 4 methylpentan-2-ol (**4**).

and during data analysis what applies especially to issue of useful analytical signal shielding or introduction of additional background. It is also beneficial from the point of view of future technology: the process as a whole potentially can be designed to be more economically efficient. It is also more feasible to scale it up to the required production yield. The gaseous stream of products is ready as such to be fractionated by temperature-controlled condensation into subsequent collectors. The catalyst itself is less prone to mechanical degradation what increases its durability necessary during time-consuming laboratory experiments or factory plant operation. Selected systems containing different supports allow tracking different surface phenomena.

There have been already described some mechanisms addressing observed gold activity, *e.g.* ref. 18 and 19. The already mentioned strong dependence of gold catalytic activity on the used support suggests Mars–van Krevelen reaction mechanism what was confirmed in the literature.[20–22] In a two-molecule reaction, one of the molecules adsorbs on the metal nanocrystal and the other on the surface of the support, but close to the interface between them. In such case, the support plays a significant role in the reaction mechanism and, thus, in selectivity and overall performance of the catalyst.

*In situ* IR spectroscopy gives insight into adsorption phenomena happening on the catalyst surface. Differential IR spectrum of the pure catalyst and exposed to vapours of volatile unsaturated carbonyl compound (we used mesityl oxide, 4-methylpent-3-en-2-one, Fig. 1, as a model molecule) shows how this organic compound is adsorbed on the catalyst surface and how it behaves in the presence of hydrogen. If chemical adsorption occurs, the spectrum will be significantly changed with respect to the spectrum for gaseous mesityl oxide and new bands will be visible.

IR spectroscopy investigation was backed-up with structural characterisation of the catalysts by electron microscopy and powder X-ray diffraction to validate the syntheses results. Additionally, the behaviour of the materials under purely reductive conditions was examined using temperature-programmed reduction.

**Table 1** Comparison of the vibrational bands positions of functional groups found in mesityl oxide and acetone adsorbed on different materials. In parentheses "(+/−#)" the shift of a band after introduction of $H_2$ (if observed) was given

| | Vibrational band positions [cm$^{-1}$] | | | | | | | |
| | $\nu(C=O)$ | | $\nu(C=C)$ | | | | | |
| Material | Broensted site | Lewis site | Broensted site | Lewis site | $\nu(-C(O)O-)$ | $\nu(O=C=C-)$ | $\nu(R_2C=C-O^{-1})$ | Reference |
|---|---|---|---|---|---|---|---|---|
| | | | | Mesityl oxide | | | | |
| Au/SiO$_2$ | 1732 (−14) | 1677 (−9) | | 1609 (−2) | | | | This work |
| SiO$_2$ | 1735 (−1) | 1678–1668 (−5) | | 1611–1607 (−1) | | | | " |
| Au/TiO$_2$ | 1708 | 1654 | | | 1539 (−1) | | 1588 | " |
| TiO$_2$ | 1701 | 1642 | | | 1550 | | | " |
| CeO$_2$ | 1714 | | | | 1589–1500 | | 1589 (+1) | " |
| HZSM-5 | 1617 | | 1557 | | | | | 37 and 60 |
| USY | 1632–1631 | 1676 | 1565 | 1604 | | | | " |
| Al$_2$O$_3$ | | 1673 | | 1603–1589 | | | | " |
| TiO$_2$ | | | | | 1600–1400 | | | 61 |
| TiO$_2$ (rutile) | | 1655 | | 1595 | | 1545, 1430 | | 32 |
| α-Fe$_2$O$_3$ | | 1665 | 1560 | 1590 | | | | 35 |
| γ-Al$_2$O$_3$ | | 1688 | | 1613 | | | | 33 |
| TiO$_2$ | | 1666 | | 1602 | | | | 34 |
| MgO$_2$ | 1710 | 1686, 1675 | | 1626 | | | 1580 | 36 |
| | | | | Acetone | | | | |
| SiO$_2$ | 1709 | | | | | | | 31 |
| TiO$_2$ (rutile) | | 1680 | | | | | | 32 |
| MgO, NiO | | | | | | 1560–1510 | | 62 |
| α-Fe$_2$O$_3$ | | 1685, 1675 | | | | | 1540 | 35 |
| γ-Al$_2$O$_3$ | | 1696 | | | | | 1596 | 33 |
| γ-Al$_2$O$_3$ | 1705–1700 | 1702–1690 | | | | | | 37 and 60 |
| TiO$_2$ | | 1702 | | | | | | 34 |

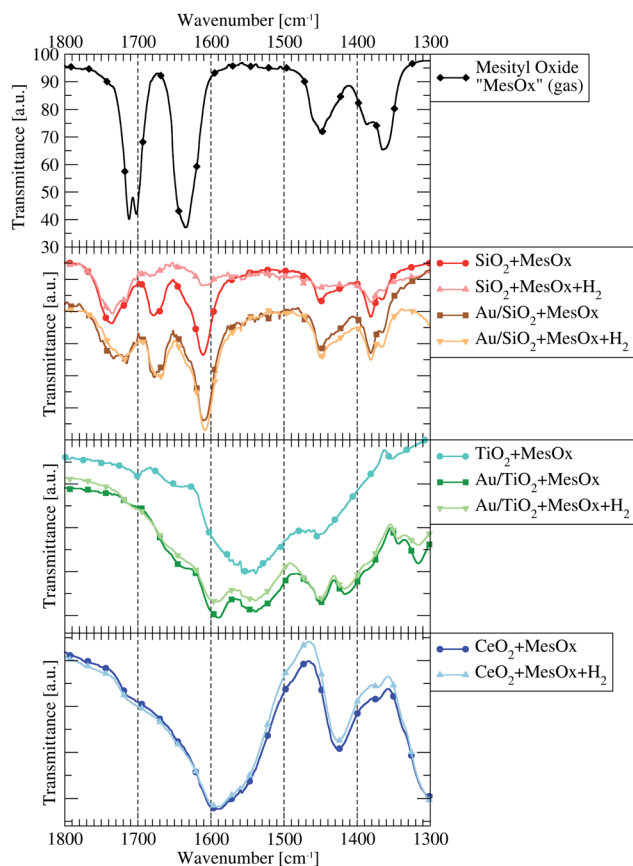**Fig. 2** The IR spectra limited to the 1800–1300 cm$^{-1}$ energy range presenting the vibrational bands of free gaseous mesityl oxide (MesOx, black line on the top plot), its derivative species (before and after introduction of H$_2$ subsequently evacuated from the system) adsorbed on the surface of catalysts (Au/material + MesOx) or pure supports (not containing gold nanoparticles; material + MesOx).
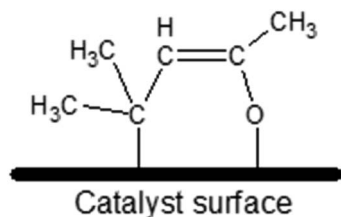


**Fig. 3** Possible schematic representation of the enolate adsorption form (also called "metallacycle" by ref. 40) of mesityl oxide on the catalyst surface – adsorption occurs thanks to binding to the surface of the oxygen atom from the carbonyl group and the β-carbon atom with respect to the carbonyl group.

Development of efficient and applicable catalytic materials shall focus on creating adsorption sites on the materials' surface that favour hydrogenation of just right functional groups to desired final products. Herewith, we provide a useful recipe how to study adsorbates on powder materials. Selected conditions can be screened readily, like temperature, reagents concentration or pressures. Equally important, we supply the method to process data and draw conclusions. Investigation of

a series of materials should finally end up in finding the optimised system working under appropriate conditions (to be established separately).

An important issue, reminded in Conclusions section, is the possible occurrence of limiting reaction steps, *e.g.* desorption of final products. Such an obstacle may cause a very promising catalyst, although able to provide right circumstances for the reagents to be transformed, to fail in supplying large quantities of the desired products at the reactor's outlet, thus, allowing the less favourable product to be obtained instead.

On balance, the results of this research show effects of interaction in which reagents, intermediate products and the catalysts surface (both the surface of the support and crystals of gold) are involved. Insights and new data on the studied catalytic systems are likely to be the crucial step towards development of this branch of chemistry and steer further research activities.

## Experimental

### Materials

Mesityl oxide (abbrev. MesOx, 99.5%, Merck KGaA) for catalytic activity tests was stored in the Schlenk flask under He. MesOx for *in situ* FTIR spectroscopy experiments was additionally distilled under N$_2$ atmosphere and was stored in the Schlenk flask under only its own vapours (*i.e.* at a diminished pressure).

The following gases: H$_2$ (99.999%, Multax S.C.), He (99.999%, Multax S.C.), N$_2$ (99.999%, Multax S.C.), Ar (99.999%, Multax S.C.), 10%$_{vol}$ H$_2$ in Ar (prepared by Multax S.C. from 99.999% purity gases), O$_2$ (99.999%, Multax S.C.) were used in all experiments.

In the catalysts syntheses the following materials were used: cerium dioxide (CeO$_2$, Austranal Praeparate), titanium dioxide (TiO$_2$, Aeroxide® P25), silica (SiO$_2$, Davison 62) hydrogen tetrachloroaurate(III) trihydrate (HAuCl$_4$·3H$_2$O, 99.9%, Alfa Aesar), sodium borohydride (NaBH$_4$, 99%, Sigma-Aldrich), sodium hydroxide (NaOH, ppa, Chempur), 1,2-ethylenediamine (H$_2$NCH$_2$CH$_2$NH$_2$, will be abbreviated by "en", ≥99.5%, Roth), diethyl ether ((CH$_3$CH$_2$)$_2$O, will be abbreviated by "Et$_2$O", ppa, Chempur), propan-2-ol (ppa, Stanlab), 25% ammonia solution (NH$_{3\ aq}$, ppa, POCH) and double-distilled water (also referred to as redistilled water).

### Catalysts syntheses

8.7%$_{wt}$ Au/CeO$_2$ (composition assessed by XRF measurements) catalyst synthesis was inspired by M. Haruta recipe[23] and M. Zielinski MSc Thesis[24] modified by the introduction of the final reduction step with NaBH$_4$.

20 ml 0.0254 M (0.82%$_{wt}$) of tetrachloroauric acid solution diluted with 330 ml of redistilled water was vigorously stirred at 500 rpm in darkness. Under constantly monitored pH value which never exceed pH = 11, it was alkalized dropwise with 51 ml of 0.05 M NaOH$_{aq}$ and was left overnight under stirring. The initially yellow solution turned into transparent. This indicated the tetrahydroxyaurate (Au(OH)$^{4-}$) complex was formed successfully. Then, 900 mg of CeO$_2$ which was
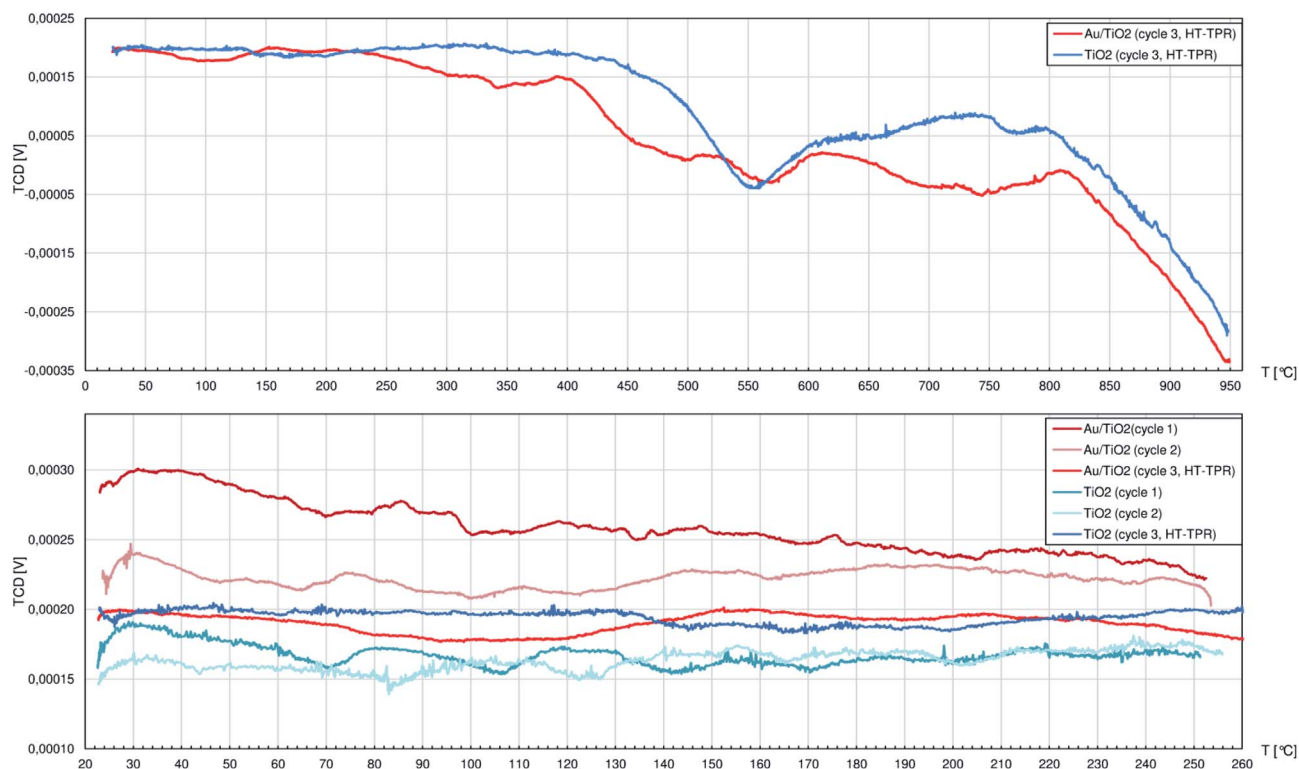
**Fig. 4** The profiles registered during temperature-programmed reduction (TPR) studies by the thermal-conductivity detector (TCD) of the 0.5%$_{wt}$ Au/TiO$_2$ catalyst and pure TiO$_2$. There were 2 cycles (cycles no. 1 and 2) of temperature ramp up to 250 °C and a 3rd cycle (cycle 3, HT-TPR) up to 950 °C. Specimens were fed with the 10%$_{vol}$ H$_2$/Ar mixture.

suspended in 50 ml of redistilled water *via* ultrasonication aided by mechanical stirring was added to the tetrahydroxyaurate complex solution. The mixture was further stirred for 2 h at 80–85 °C. After cooling the mixture down to 0 °C, 58 mg of NaBH$_4$, dissolved in 20 ml of 0.1 M NaOH$_{aq}$, was added dropwise. It resulted in immediate colour change into purple. The mixture was subsequently stirred for another 12 h in room temperature. Then, the catalyst was filtered and rinsed 15 times with redistilled water until no chlorine anions were detected. It was finally dried overnight under vacuum in 40 °C. A ready-for-use catalyst was stored in darkness in a desiccator.

0.5%$_{wt}$ Au/TiO$_2$ catalyst synthesis was also inspired by M. Haruta recipe[23] and followed the method described in M. Zielinski MSc Thesis[24] which did not include the final reduction step with NaBH$_4$, but assumed spontaneous reduction of gold cations by contact with air during drying of the catalyst at diminished air pressure.

To obtain approx. 1800 mg of the material, 40 ml 0.0254 M (0.82%$_{wt}$) of HAuCl$_4$ solution diluted with 337 ml of redistilled water was vigorously stirred at 600 rpm in darkness. While the pH value was on-line monitored and never exceeded 11, gold complex with hydroxyl groups was formed by alkalisation with 100 ml of NaOH$_{aq}$ added dropwise followed by stirring of the whole solution overnight. The solution turned from yellow into transparent. Later, it was poured into suspension containing 1800 mg of TiO$_2$ in 100 ml of redistilled water stirred at 500 rpm. The resulting constantly stirred mixture was heated to 80–85 °C

and maintained in this temperature range for 3 h. The suspended TiO$_2$ powder having immobilised on its surface the gold hydroxy-complex was filtered and rinsed 10 times with redistilled H$_2$O, while maintaining 50 °C, until no chlorine anions were detected. It was finally dried for 48 h under diminished air pressure at 40 °C. A ready-for-use catalyst was stored in darkness in a desiccator.

10.0%$_{wt}$ Au/SiO$_2$ catalyst synthesis recipe was based on the idea of Y. L. Lam and M. Boudart[25] which was applied so that only gold containing catalyst was obtained (originally Au–Pd alloyed catalyst's active phase was obtained). Gold precursor was prepared according to original B. P. Block and J. C. Bailar[26] recipe which was re-examined by W. J. Louw and W. Robb[27] and optimised by K. Kitada.[28]

Solutions of 1 g of hydrogen tetrachloroaurate(III) trihydrate in 10 ml of diethyl ether and 1 ml of 1,2-ethylenediamine in 5 ml of Et$_2$O were mixed. A gummy yellow precipitate was formed. Following 30 min of refluxing, the solvent was evaporated under diminished pressure. An orange solution of the product was obtained after addition of approx. 10 ml of water. Following addition of approx. 90 ml of propan-2-ol a yellowish precipitate was formed and subsequently filtered. Crystallization of di(ethylenediamine)gold chloride from water and propan-2-ol mixture was repeated resulting in white powder which was dried overnight under vacuum at 40 °C. Recrystallization was applied every time before using the gold complex in catalyst's synthesis.
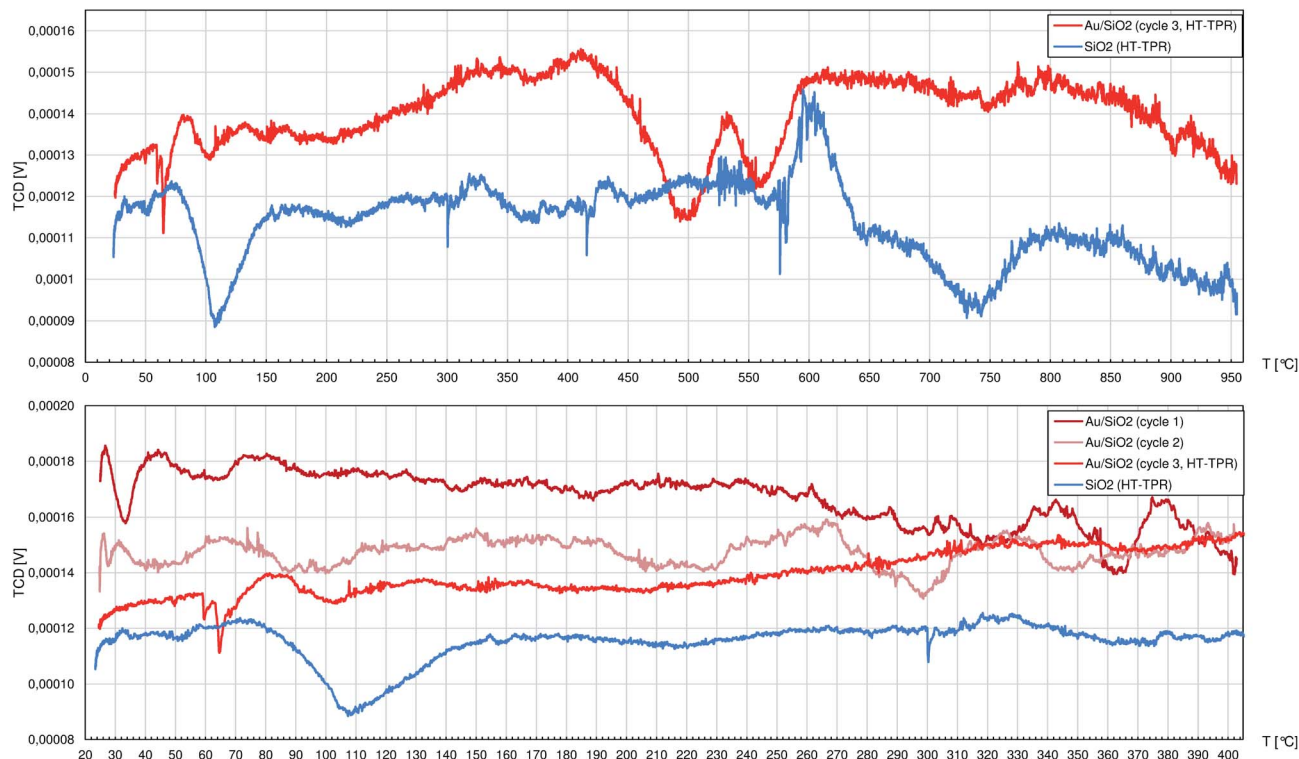
**Fig. 5** The profiles registered during temperature-programmed reduction (TPR) studies by the thermal-conductivity detector (TCD) of the 10.0%$_{wt}$ Au/SiO$_2$ catalyst and pure SiO$_2$. In the case of the catalyst, which first underwent the activation process (see the Experimental section), there were 2 cycles (cycles no. 1 and 2) of temperature ramp up to 400 °C and a 3rd cycle (cycle 3, HT-TPR) up to 950 °C. Pure SiO$_2$ was subjected only to one cycle up to 950 °C. Specimens were fed with the 10%$_{vol}$ H$_2$/Ar mixture.

All of the following steps were performed in darkness. In order to prepare 1000 mg of the catalyst, 900 mg of SiO$_2$ was suspended in 0.4 ml of 25% ammonia solution diluted with 50 ml of water resulting in pH ∼ 11. The mixture was stirred at 500 rpm. 215 mg of fresh di(ethylenediamine)gold chloride dissolved in 50 ml of water (transparent solution) was added dropwise to silica suspension. The slurry was heated up to 70 °C. Following 1 h when the temperature never dropped below 68 °C, the mixture, which turned into yellow, was filtered under diminished pressure, rinsed 10 times with water and dried overnight under vacuum. A yellow powder was obtained.

Before performing any experiments, the catalyst was activated in 20 ml min$^{-1}$ flow of H$_2$ for 80 min in 50 °C, then 160 min in 100 °C and finally 400 min in 150 °C. The activation procedure aimed at reducing the gold cation complex anchored to SiO$_2$ surface to gold particles closely bound with the support surface. At the same time, the 1,2-ethylenediamine ligand was released as possibly free ammonia (NH$_3$) and ethane (C$_2$H$_6$).

**The catalytic activity tests**

The catalysts' chemical activity was checked in the reaction setup based on the U-shaped glass reactor resembling the model of the Plug-Flow Reactor (PFR). The catalyst's bed (approx. 100 mg depending on the material's bulk density) was formed as a thin layer of powder uniformly distributed over the 15 mm fused silica disk welded into the reactor's walls. The whole reactor was placed in the furnace that was slowly (2 °C min$^{-1}$) heated from 145 °C up to 350 °C and all the tubing outside the furnace through which MesOx vapours flew were maintained at 145 °C (*i.e.* at lowest reliable temperature at which neither MesOx nor its hydrogenation derivatives condense).

16.93 µl min$^{-1}$ of liquid MesOx (equivalent to 3.33 ml min$^{-1}$ flux after evaporation to the gas phase) was dosed using a syringe pump (New Era Pump Systems 1000 X-ES) into the gas stream formed by mixing 4 ml min$^{-1}$ of H$_2$ with 14 ml min$^{-1}$ of He at 1 atm. The 20% H$_2$ excess was provided to allow detection of fully-hydrogenated products in case of full conversion of MesOx.

Right behind the glass reactor, the quartz capillary sampling the outlet stream to the mass spectrometer (MS, HPR-20 from Hiden Analytical Ltd.) was attached. The quadrupole MS with 2 detectors (Faraday cup and secondary electron multiplier covering together pressure range from $10^{-13}$ to $10^{-5}$ bar) provided on-line insight into the hydrogenation reaction outcome up to 200 amu. The unused reactant and all products were condensed and collected before the exhaust.

To avoid unwanted condensation/polymerisation reactions at highest temperatures and maintain stable long-time activity of the studied materials, the *in situ* IR experiments were carried out at $T \leq 300$ °C (self-ignition temperature of *e.g.* MesOx in air is 344 °C (ref. 29) and of 4-methylpentan-2-ol is 305 °C (ref. 30)). The MS spectra analysis results were validated by gas
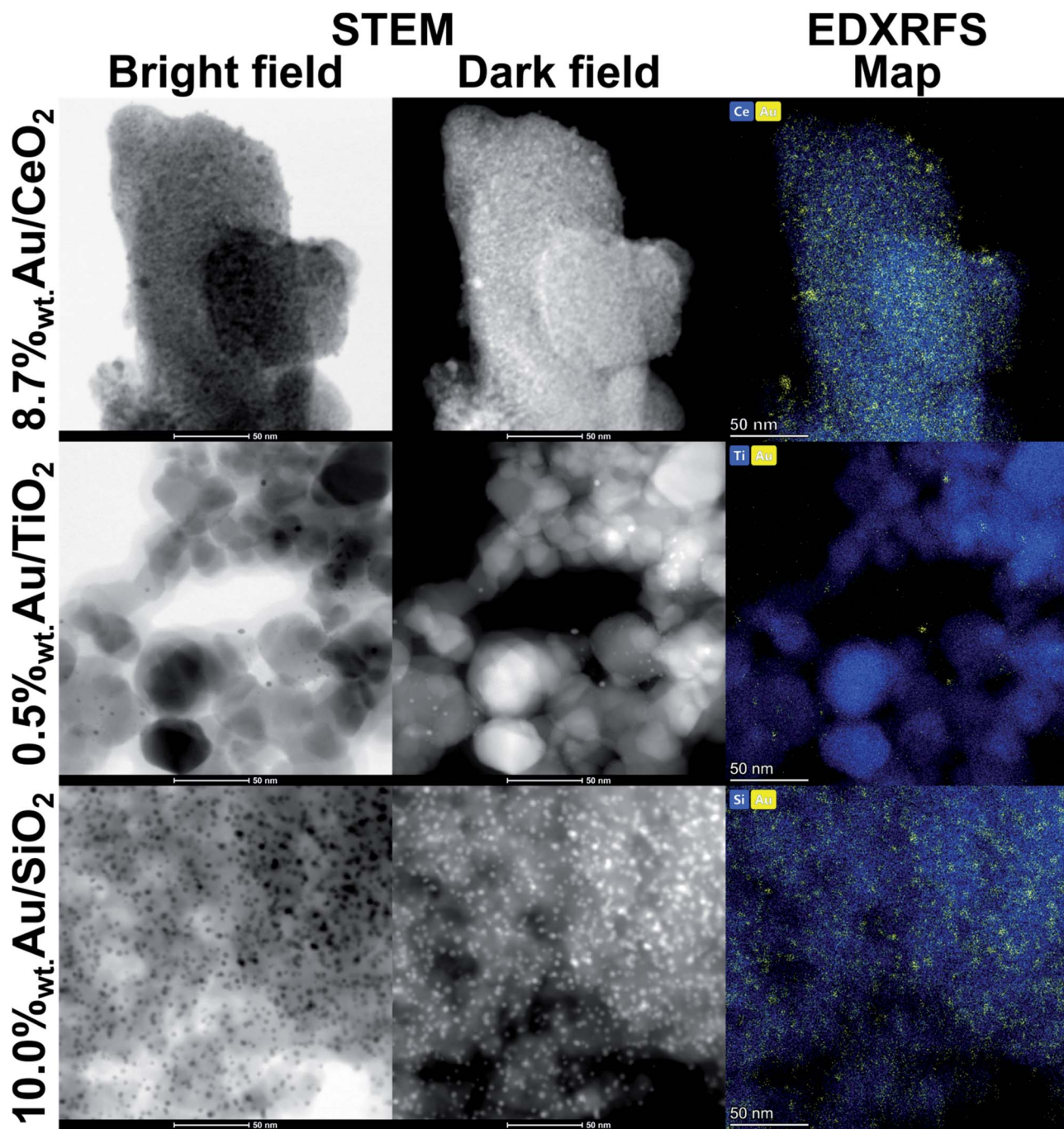
**STEM**
**Bright field** | **Dark field**
**EDXRFS Map**

Fig. 6 STEM bright and dark field images accompanied by the corresponding EDXRFS maps presenting the morphologies of 8.7%$_{wt}$ Au/CeO$_2$, 0.5%$_{wt}$ Au/TiO$_2$ and 10.0%$_{wt}$ Au/SiO$_2$ catalysts while differentiation between AuNPs and support is facilitated by composition maps limited to show distribution of only Au, Ce, Ti and Si elements.

chromatography (Agilent 8860, column ZB-WAX) analysis of the condensate collected only at 280 °C for 1 h (see ESI†).

### In situ infrared spectroscopy

Fourier-transformed infrared (FTIR) spectra in transmission mode were acquired using the Nicolet 6700 spectrometer equipped with a in-house made of quartz glass in situ measurement chamber with CaF$_2$ windows.[24,63-65] The chamber was connected to the tube furnace localised directly above the chamber. The specimen (thin pellet made of grinded and pressed powder) mounted in the quartz holder was lifted between the chamber for the spectrum acquisition and the furnace for adsorption/desorption of gases at a given temperature.

The setup was connected to a vacuum-gas system. Oil diffusion pump with a double liquid nitrogen trap provided vacuum approx. $2 \times 10^{-5}$ mbar. H$_2$ was stored in a glass tank and was dosed to the catalyst pellet in the furnace by adjusting the pressure to 50 mmHg

**Table 2** Structural parameters of the phases identified in the diffraction patterns of the $8.7\%_{wt}$ $Au/CeO_2$, $0.5\%_{wt}$ $Au/TiO_2$ and $10\%_{wt}$ $Au/SiO_2$ catalysts. The last figure regression error is given in parenthesis

| Material | Crystal phase | Index | Lattice parameters | | $\%_{wt}$[a] | Size[b] [nm] | Strain–stress $(\varepsilon)$ factor |
| --- | --- | --- | --- | --- | --- | --- | --- |
| | | | $a$ [Å] | $c$ [Å] | | | |
| $8.7\%_{wt}$ $Au/CeO_2$ | $CeO_2$ | 1 | 5.4202(1) | — | 56.1(4) | 16.0(4) | 0.00111(2) |
| | | 2 | 5.4229(3) | — | 27.4(4) | 6.5(2) | 0.00391(11) |
| | Au | | 4.0823(2) | — | 16.4(1) | 23.0(20) | 0.0020(10) |
| $0.5\%_{wt}$ $Au/TiO_2$ | $TiO_2$ (anatase) | 1 | 3.7908(2) | 9.5228(7) | 61.7(40) | 20.6(10) | 0.00045(3) |
| | | 2 | 3.7935(5) | 9.499(4) | 24.5(40) | 10.7(7) | 0.00186(16) |
| | $TiO_2$ (rutile) | | 4.6015(3) | 2.9632(2) | 13.6(2) | 27.2(10) | 0.00(6) |
| | Au | | 4.0780[c] | — | 0.2(40) | 4.6(17) | n/a[d] |
| $10.0\%_{wt}$ $Au/SiO_2$ | Au | | 4.0776(45) | — | 100.0 [e] | 3.5(12) | 0.01(2) |

[a] According to Rietveld refinement based on the unit crystal cell mass. [b] Volume-weighted average crystallite size calculated according to Laue[59] from integral breadth of the fitted Voigt function. [c] The lattice parameter $a$ of gold was constrained to the reference value,[50] because the amount of gold ($0.5\%_{wt}$) was too small to yield a stable fit of the model phase to the experimental data. [d] The scattering contribution of gold to the experimental line profile was too small to allow differentiation between the peak broadening originating from size and strain–stress, hence the integral breadth was attributed wholly to size-related effects. [e] The scattering contribution of amorphous $SiO_2$ has not been assessed in terms of silica content.

in the *in situ* setup isolated from the vacuum system at that moment. Freshly distilled MesOx was dosed from the Schlenk flask attached directly to the glass apparatus.

Before the main part of *in situ* FTIR experiment, each sample (the catalyst or the pure oxide support) pellet was heated at 300 °C under vacuum for at least 1 h. The 300 °C temperature was maintained during later stages of the experiment. The background spectrum was the one collected for an empty chamber and it was subtracted from all subsequent spectra. The fresh preheated sample was lowered from the furnace to the chamber to acquire (after the sample cooled down) the spectrum corresponding to the clean catalyst's surface state "as it was". Then, the MesOx vapours (partial pressure equalled saturation at room temperature) were supplied for 5 min to the previously vacuum-pumped system and the sample was placed at that time in the furnace set to 300 °C. Next, the system was vacuum-pumped for 15 min and the spectrum of MesOx adsorbed at the catalyst's surface was acquired. Later, 50 mmHg of $H_2$ was supplied for 5 min to the sample with adsorbed MesOx, placed in the furnace. After that time, a spectrum corresponding to the absorbates state under $H_2$ atmosphere was acquired. Finally, the system was vacuum-pumped again for 15 min and the spectrum of adsorbates remaining at the catalyst's surface was collected.

Thus, sets of 3 valuable spectra were obtained, corresponding to: (1) pure sample; (2) sample with adsorbed MesOx; (3) sample with adsorbed species after being in contact with $H_2$. Data analysis was based on differential spectra, *i.e.* after spectrum no. 1 was subtracted from spectra no. 2 and 3 to reveal the contributions from the adsorbates.

**Temperature-programmed reduction**

TPR measurements were carried out in a glass apparatus equipped with the U-shaped fixed bed quartz glass reactor, with

the TCD detector and using $10\%_{vol.}$ $H_2$ in Ar as the carrier gas. The catalysts and their pure supports underwent the same experimental procedure. At first, the samples were flushed with pure Ar for 1 h, after which the carrier gas was changed to $H_2$/Ar mixture. Then, there were 2 repetitive cycles of temperature ramp (10 °C min$^{-1}$) up to 250 °C (each heating cycle was followed by the cooling step down to room temperature under pure Ar). These cycles were intended to show whether low-temperature and instantly reversible interaction of the sample with gaseous $H_2$ can be observed. Finally, the heating cycle up to 950 °C was performed to provide comprehensive characterisation of the materials' behaviour under reducing atmosphere.

In the case of $Au/SiO_2$ catalyst, prior to carrying out the main TPR cycle, the fresh as-synthesised sample still containing Au–en complexes was subjected to the activation procedure *in situ* in the TPR apparatus without acquisition of the TCD signal. For the pure $SiO_2$ sample, only one TPR cycle from room temperature to 950 °C was performed due to very inert character of $SiO_2$ showed in the preliminary studies.

**Transmission electron microscopy**

*Ex situ* Transmission Electron Microscopy (TEM) studies in the scanning mode (STEM) were conducted on TALOS F200X microscope with X-FEG gun operated at 200 keV and equipped with Super X EDS system used for elemental composition mapping.

## Results and discussion

### Catalytic activity

Each of the pure supports was expected to be inactive in R-(V) ABUCC reaction which indeed is the case. However, pure $CeO_2$ shows, judging by the selected signals (refer to Fig. S1 in ESI†) in the MS spectrum acquired in function of the

temperature (Fig. S2†) small and rapidly decreasing activity towards conversion of MesOx into a SK (saturated ketone, methyl-isobutyl ketone, 4-methylpentan-2-one). It is assumed, that such an observation is possible due to presence of residual adsorbed components of air that cannot be removed at 145 °C, which are the places of adsorption and the starting point for the reaction. It is doubtful that introduction of $H_2$/He mixture to the reactor prior to starting dosing MesOx can explain the behaviour of $CeO_2$, because no interaction between $H_2$ and pure $CeO_2$ was spotted at 145 °C in TPR studies (described later in the text).

Comparing the catalysts performance by GC analysis of R-(V) ABUCC reaction products collected over 1 h at 280 °C (Table S1†), $8.7\%_{wt}$ Au/$CeO_2$ proves to be the most active system. It converts almost 25% of α-MesOx from the stream mainly into SK (yield approx. 15%). 0.5% Au/$TiO_2$ catalyst converts over 16% of α-MesOx, but mainly into its β isomer, and only about 3.5% of SK is formed. Similarly, $10.0\%_{wt}$ Au/$SiO_2$ converts only 9.7% of α-MesOx into, almost equal amounts of, SK (4.7%) and β isomer (5%).

Performance of the catalysts was not optimised because the chemical tests in the glass reactor were carried out to provide a reference point for the *in situ* FTIR studies (described below) and the experiments in the *in operando* PXRD chamber that are planned to be carried out as the next research step. Another, possibly important, factor was that a thin layer of material uniformly distributed over the fixed bed in the glass reactor had to be applied. This was crucial to maintain the differential glass reactor model and prevent any mass transport inside the sample layer, especially leading to a creation of concentration profile of gold particles AuNPs towards the direction of gas flow.

### *In situ* IR spectroscopy

The *in situ* collected FTIR spectra show that both: the support type and lack or presence of AuNPs are crucial factors determining which adsorbed forms of MesOx can be found on the surface of the studied material. After $H_2$ is introduced to the system, some of the observed bands have their peak-tops shifted by a couple of wavenumbers ($cm^{-1}$) what may be a trace of some intermediate products of hydrogenation of MesOx. A summary of the results described below and comparison with the literature can be found in Table 1.

Unfortunately, it was impossible to acquire any meaningful spectra in the case of $8.7\%_{wt}$ Au/$CeO_2$ catalyst. The catalyst has deep purple colour and the thin pellets made of its powder were either too fragile to withstand the mounting procedure in the quartz holder or they were completely not transparent for the IR laser light, thus, almost no beam intensity could be registered by the detector in whole energy range regardless of the spectrometer configuration and settings.

Similarly, the pure $TiO_2$ powder allowed preparing pellets that never survived beyond the MesOx adsorption phase, so no spectrum was acquired for $H_2$-influenced MesOx adsorbed on $TiO_2$, even though numerous attempts were embarked.

Although the IR spectra were acquired from 4000 $cm^{-1}$ to 1300 $cm^{-1}$ the interesting bands responsible for C–O and C–C bonds vibrations as well as –$CH_3$ bending modes and $\delta_{CH}$

deformation vibration of hydrocarbon groups can be found in the range between 1800–1300 $cm^{-1}$. Above 3000 $cm^{-1}$ all bands characteristic for MesOx and its derivatives overlay with the very broad and intense bands corresponding to –OH vibrations. The $^{sp^2}$C–H and $^{sp^3}$C–H vibration bands in the 3000–2900 $cm^{-1}$ energy range do not provide clear conclusions about neither MesOx adsorption state nor interaction with $H_2$, because mainly only the intensity of the bands change. Hence, these mentioned energy ranges are excluded from the discussion presented below.

The spectrum of pure MesOx in the gas phase (vapour pressure equalled saturation at room temperature), presented in Fig. 2, exhibits sharp bands in the 1800–1300 $cm^{-1}$ range and a couple of overlaying bands of weaker intensity in the 3000–2900 $cm^{-1}$ range. The latter correspond to stretching vibrations of the $^{sp^2}$C–H and $^{sp^3}$C–H bonds. The former, between 1500 $cm^{-1}$ and 1300 $cm^{-1}$, originate from the methyl groups bending modes and deformation vibration of hydrocarbon bonds.[31–34] Additionally, between 1800 $cm^{-1}$ and 1600 $cm^{-1}$, there are signals connected to stretching vibrations of the carbonyl group (1702 $cm^{-1}$ and 1712 $cm^{-1}$) and to stretching vibration of the $^{α}$C=$^{β}$C double bond.

The most chemically active catalyst from the studied set was the one based on $CeO_2$ support. The dominant form of adsorbed MesOx found on the bare $CeO_2$ surface not decorated with AuNPs is the enolate form (*i.e.* adsorption through the oxygen atom and the β-carbon atom, Fig. 3) as evidenced by band peak-top at 1589 $cm^{-1}$ before and 1590 $cm^{-1}$ after introduction with $H_2$ (ref. 33, 35 and 36, Fig. 2). Additionally, the right-hand shoulder ranging till 1500 $cm^{-1}$ suggests that adsorption of MesOx yielded species containing carboxylic groups[33] which could be formed only by adsorption supported by oxygen atoms or hydroxyl groups of the materials surface. The small hump observed at 1714 $cm^{-1}$ suggests that also adsorption through carbonyl group to the Brønsted acidic centre occurs.[36,37] With regard to observation of the dominant enolate form, the spectrum profile for wavenumbers smaller than 1500 $cm^{-1}$ changes significantly, reflecting new vibrational constants of bending of the –$CH_3$ groups neighbouring the β-carbon atom by forming two bands centred around 1371 $cm^{-1}$ and 1423 $cm^{-1}$[37]

Especially the enolate form, but also the carboxylic one, are expected to be very active species due to serious relocation of the electron density across the adsorbed molecule. Thus, adsorption of MesOx in these forms on the surface supposedly favours hydrogenation of: (1) $^{α}$C=$^{β}$C double bond to saturated ketone (what was clearly observed by GC and MS); (2) C=O carbonyl group to allyl alcohol (only traces of AA were detected by MS); or (3) regrouping of double bonds upon desorption without hydrogenation to create iso-mesityl oxide (4-methylpentan-4-en-2-one).

$TiO_2$ alone has clear preference to support MesOx adsorption by incorporation of surface oxygen atoms as evidenced by the carboxylic group vibrational band centred at approx. 1550 $cm^{-1}$ (ref. 33, Fig. 2). Additionally, the two bands at 1701 $cm^{-1}$ and 1642 $cm^{-1}$ point to possible adsorption of the MesOx carbonyl group to acidic centres, Broensted and Lewis type respectively,[36,37] present on the $TiO_2$ surface. The small acidity of $TiO_2$

was utilised during the Au/TiO$_2$ catalyst synthesis to attach Au(OH)$_x^{3-x}$ complex ions to the oxide surface through ion exchange. In the 1500–1300 cm$^{-1}$ range, only a C–H deformation band at 1454 cm$^{-1}$ can be observed while methyl group bending modes remain invisible.

On the contrary to pure TiO$_2$, the Au-decorated surface of titania shows ability to stabilise the adsorbed MesOx in the enolate form due to which a band at 1588 cm$^{-1}$ can be spotted. Correspondingly to the formation of enol-type species, bands at wavenumbers below 1450 cm$^{-1}$ are observed similarly to the case of pure CeO$_2$. Au/TiO$_2$ spectra still exhibit features characteristic for pure TiO$_2$, *i.e.* interaction of the MesOx carbonyl group with acidic centres of the surface (1708 cm$^{-1}$ and 1654 cm$^{-1}$) and with surface oxygen atoms taking part in carboxyl group formation (1539 cm$^{-1}$).

Samples containing SiO$_2$ yield much different IR spectra demonstrating basically 3 types of MesOx adsorption to acidic sites: the H-bonded (Broensted site) and electron-donating (Lewis site) carbonyl group corresponding to 1735 cm$^{-1}$ and 1668–1678 cm$^{-1}$ bands, respectively; and the C=C double bond adsorbed also to a Lewis site as indicated by the 1607–1611 cm$^{-1}$ band.

Pure silica was unable to hold MesOx on its surface after H$_2$ was introduced to and evacuated from the system. On the other hand, the deposition of gold helped keeping the MesOx on the surface of the catalyst under H$_2$ atmosphere (Fig. 2) and, furthermore, the bands observed at 1609 cm$^{-1}$, 1677 cm$^{-1}$ and 1732 cm$^{-1}$ shift to lower wavenumbers by 2–14 cm$^{-1}$. The change of strength of the carbonyl group and $^\alpha$C=$^\beta$C double bonds may be interpreted in terms of ability of ultrasmall (<5 nm) AuNPs to interact with hydrogen[38,39] and supplying its active forms to the adsorbed MesOx. At the same time, the bands connected to vibration of methyl groups remain unchanged. They closely resemble the band structure of gaseous MesOx what is expected with regard to adsorption of only the conjugated bonds on the acidic sites.

Pure TiO$_2$, as well as other pristine supports, shows no catalytic activity towards neither hydrogenation nor isomerisation of MesOx at temperatures up to 350 °C, but the Au-containing systems demonstrate clear conversion. Additionally, comparing Au/CeO$_2$ and Au/TiO$_2$ results, the conclusion can be drawn that, in terms of hydrogenation of MesOx to SK and, possibly, also other derivatives under optimal conditions, the enol-type of adsorption of MesOx would be favourable over adsorption leading to formation of a carboxyl group. The case of Au/SiO$_2$ catalyst adds also the observation that weakening of the C=C double bond through its adsorption to a Lewis acidic site is sufficient for its hydrogenation provided that the system can supply active forms of hydrogen (as gold-decorated supports do). Although the 1609–1607 cm$^{-1}$ band corresponding to C=C adsorption is most prominent in the SiO$_2$-based systems, such adsorption type cannot be ruled out in the cases of other catalytic systems.

In general, in this work the term "Lewis acidic site" covers broad range of species that are electrophilic, just to mention: oxygen vacancies present in the catalysts' oxide supports, and gold which, as a transition metal, has its d-band in principle able to accept/exchange electrons with C=C or C=O bonds.[40,41]

## Temperature-programmed reduction

The TPR studies on CeO$_2$ and Au/CeO$_2$ have been once published by us elsewhere.[42] In brief, we proved that Au/CeO$_2$ catalyst, unlike pure CeO$_2$, is able to cyclically adsorb and immediately release hydrogen in temperatures below approx. 250 °C. Attention was also put on the capability of ceria itself to adsorb carbon dioxide from air. The physically bound CO$_2$ can be desorbed below 150 °C, but only above 300 °C the strongly adsorbed CO$_2$ is released after just thermally induced decomposition to CO (2 peaks at 325 °C and 670 °C proved by MS analysis). As the catalyst contains AuNPs facilitating adsorption of hydrogen, different H$_x$CO$_y$ species are presumably formed.[43–45] Hence, carbon oxides are released from the Au/CeO$_2$ surface at higher temperatures as evidenced by peaks shifted to 484 °C and 805 °C.

The TPR profiles of pure and Au-decorated CeO$_2$ are, naturally, the sum of CO$_2$ desorption-related phenomena as well as phase reduction of ceria. The latter starts at the surface, judging by the peak at 520 °C, to be followed by bulk reduction represented by the peak at 880 °C.[44] The Au/CeO$_2$ catalyst shows similar behaviour, although H$_2$ consumption for surface reduction starts as early as from 300 °C and the bulk transformation yields peak at 810 °C.

Comparing to materials containing CeO$_2$, the TPR profiles of the other materials show peaks that are approx. an order of magnitude smaller (considering both peak height and area) while similar masses of samples were used. Thus, the marked capability of CeO$_2$ to interact with and store hydrogen (*e.g.* [ref. 46]) necessary to reduce MesOx is confirmed.

Below 400 °C the TPR profile of pure TiO$_2$ (Fig. 4) shows only peaks with negligible height: during the 1st cycle at 71 °C, 107 °C, 143 °C and 171 °C and during the 2nd cycle only 3 peaks at 84 °C, 125 °C and 202 °C. Unlike CeO$_2$, titania does not adsorb large quantities of air components, so at relatively low temperatures only little amounts of thermally desorbed gases were released to the H$_2$/Ar stream slightly diluting it. The first strong peak is observed in the 3rd cycle at 554 °C and corresponds to slow release of oxygen ions as H$_2$O from the rutile structure caused by H$_2$ adsorbed on the oxygen vacancies V$_O^{++}$.[47] The more V$_O^{++}$ are formed, the more O$^{2-}$ anions diffuse outwards from the inner titania structure, and the process seems to behave like an autocatalytic one. While the reduction proceeds smoothly between approx. 600 °C and 800 °C, it is followed by heavy increase of hydrogen consumption that is interrupted at 950 °C after the TPR system reaches its technological limits. Above approx. 750 °C anatase is expected to transform to rutile[48] which easily undergoes the same mechanism as described above, adding its contribution to the TPR curve.

Similarly to pure TiO$_2$, the Au/TiO$_2$ catalyst can be considered as rather not influenced by hydrogen atmosphere up to 210 °C when the H$_2$ consumption starts to increase until the first peak top at 342 °C. Later above 400 °C, numerous peaks are

identified, namely at: 456 °C, 496 °C, 569 °C, 700°, 745 °C and above 810 °C the reduction process largely consuming $H_2$ could continue well above 950 °C.

AuNPs on the $TiO_2$ clearly facilitate its interaction with hydrogen. The reduction passes through more stages that also happen at approx. 150 °C lower temperatures comparing to pure titania. The improved affinity of Au/$TiO_2$ system to $H_2$, like the augmented adsorption of MesOx on Lewis sites, can both rely on better electron-accepting properties of $TiO_2$ in the proximity of AuNPs.

$SiO_2$ allowed to collect a very noisy but flat TPR profile (Fig. 5) with only 3 peaks at 108 °C, 604 °C and 737 °C featured by poor signal-to-noise ratio. Pure $SiO_2$ during heating, even under $H_2$ atmosphere, can release mainly adsorbed water (not visible by TCD detector due to cold trap mounted in the tubing) and residual adsorbed air components, but the observed peaks are of little importance to the R-(V)ABUCC reaction.

The TPR experiment on the Au/$SiO_2$ catalyst had to be preceded by the post-synthesis activation process (decomposition of gold–ethylenediamine complex with crystallisation of AuNCrs followed by burning of the organics residuals) performed *in situ*. Thus, the 1st and 2nd cycles finished at 400 °C regarding the temperature reached in the last stage of activation. Any peaks that can be eventually spotted in these profiles were insignificant (*i.e.* they can not be clearly described because of comparably high alternations of the baseline). During the 3rd cycle, 2 peaks between 450 °C and 600 °C are noted. On the absolute scale they have to be regarded as weak, but there are no corresponding peaks in the TPR profile of pure $SiO_2$. Indeed, the observed in this case $H_2$ consumption is minute and occurs beyond the catalyst working conditions for R-(V)ABUCC reaction, hence it is excluded from further analysis.

### Morphology and crystal structure

Transmission electron microscopy (TEM) was used in the scanning mode (STEM) to investigate the morphology and elemental composition (by means of energy-dispersive X-ray fluorescence spectroscopy, EDXRFS) of the catalysts (Fig. 6).

AuNPs deposited on $SiO_2$ have narrow size distribution and virtually all observed particles are smaller than 5 nm. The PXRD diffraction data provides estimation of the volume-weighted crystallite size around 3.5 nm (Table 2). AuNPs are also uniformly dispersed on the $SiO_2$ surface. This feature has to be attributed to the synthesis method based on the immobilisation of $Au^{3+}$–ethylenediamine complex on the catalyst support. Thermal decomposition of the AuNPs precursor assisted by simultaneous reduction of gold ions to metallic form by $H_2$ provides instant seeding of AuNPs in the whole volume of the prospective catalyst. Thus, growth of bigger crystals at the expense of formation of numerous smaller ones is inhibited.

Application of ethylenediamine as the $Au^{3+}$ ligand was not possible in syntheses using other supports due to insufficient binding of the AuNPs precursor to the $CeO_2$ and $TiO_2$ surface. For these supports, the ion exchange of hydroxyl groups between the oxide surface and $Au(OH)_4^-$ was utilised. Although the method can be considered efficient for synthesis of Au/$CeO_2$

catalyst, limited success was observed for Au/$TiO_2$ system. The Au loading on $TiO_2$ surface was limited to 0.5%$_{wt}$, but small AuNPs were obtained, similarly to the $SiO_2$-based catalyst. That small content of Au prevented fully free fitting of the diffraction profile and the *a* lattice parameter of gold had to be constrained to ideal 4.078 Å.

Commercially available $TiO_2$ under the name "Aeroxide" consists of 2 titania phases: anatase and rutile. The diffraction peaks exhibit marked broadening of the peaks' bases which resulted in using 2 fractions of anatase phase to fit the experimental scattering profile. The lattice parameters *a* and *c* of the phases differ by only 0.3 pm, but the average-by-volume crystallite size varies by the factor of 2, namely the diameters are established around 20 and 10 nm (Table 2).

The Au/$CeO_2$ catalyst contains AuNPs with broad distribution of sizes, although their desired uniform dispersion is maintained as in the cases of other catalysts. The overview presented in Fig. 6 shows that the majority of AuNPs is smaller than 10 nm, *i.e.* that fraction does not differ much from gold crystals deposited on other supports. However, occasionally larger particles can be spotted which is an important factor in the diffraction patterns analysis. Diffraction is a phenomenon that heavily depends on the volume of the coherently scattering object, yet occurrence of large crystals shifts the volume-weighted average crystallite size to above 20 nm (Table 2).

The established $CeO_2$ and Au lattice parameters were found to differ by only approx. 0.5–1 pm from the reference values: 5.411 Å and 4.078 Å, respectively.[49] The slight expansion of $CeO_2$ structure could be explained by the deviation of the stoichiometry. $CeO_{2-x}$ (as better to be referred to), especially the nanocrystalline powder, was reported to expand the volume of the unit cell with loosing oxygen ions due to larger $Ce^{3+}$ ionic radius that even compensates the formation of oxygen vacancies.[50] The issue has been also covered by us elsewhere.[42] The increase of Au lattice parameter resulted from the residual intensity between the 1 1 1 and 2 0 0 diffraction peaks not included in the Au fcc crystal model. This additional scattering contribution was characteristic for multiply-twinned particles.[51–53] When 5 tetrahedra crystallites form one particle, that particle has 5-fold symmetry (a, possibly truncated, decahedron is obtained) along [110] direction, but the crystal lattices of the building crystallites have to be strained in order to connect all the crystallites boundaries.[54] This strain has to be applied mainly to the (111) and (200) planes (parallel to [110] direction) what leads to decreasing the $2\theta$ angle difference between the 1 1 1 and 2 0 0 peaks, hence the fcc model always leaves the residual not described intensity in the diffraction pattern.

In general, decahedral nanoparticles in TEM images resembled a much more common fcc crystals ordering and only when aligned with the [110] direction perpendicular to the imaging plane it might be possible to see the twinned single-crystal domains wrapped around the 5-fold symmetry axis.

## Conclusions

Our research results showed the possibility of investigating the adsorbed forms of reactants on the surface of heterogeneous

powder catalyst and connecting the observed catalytic activity with the way the material interacts with hydrogen, thus allowing reduction of organic compounds. To achieve our goal, we employed *in situ* infrared spectroscopy (IR) in transmission mode, temperature-programmed reduction (TPR) studies as well as electron microscopy (TEM) and X-ray diffraction (PXRD) for morphology and crystals structure determination.

Presence of gold nanoparticles was proved to be essential when they are supported on the selected for this research oxides for the reduction of α,β-unsaturated carbonyl compounds. As proved by the IR spectra, mesityl oxide (MesOx) adsorbs on pure oxides but remains insensitive to hydrogen atmosphere, Au seems to us to be involved mainly in adsorption and activation of $H_2$ molecule. Hence, increased hydrogen consumption in TPR studies was observed at lower temperatures than for pure ceria, titania and silica. Immediately reversible after gas atmosphere change binding of hydrogen by $Au/CeO_2$ system was spotted even below 100 °C. Both $TiO_2$- and $SiO_2$-based catalysts additionally benefited from their surface decoration with Au. In the former case, enolate derivatives of MesOx were found adsorbed on the surface on the contrary to observations made for pure $TiO_2$. The latter example revealed the direct interaction between MesOx-related species and Au evidenced by more stable and longer-lasting adsorption of MesOx on the $Au/SiO_2$ catalyst surface.

We have identified 3 most desirable adsorption forms of MesOx on the catalysts surface that allow reduction of MesOx, in our research to a saturated ketone (namely 4-methylpentan-2-one, also called methyl-isobutyl ketone), that is:

• Adsorption on $CeO_2$ and $TiO_2$ through the oxygen atom from the carbonyl group and the β-carbon atom with respect to the original carbonyl group;

• Adsorption leading to formation of species containing a carboxyl group formed by incorporation of the hydroxyl group available on the $CeO_2$ and $TiO_2$ surfaces;

• Adsorption of the $^\alpha C=^\beta C$ double bond to a Lewis acidic site that weakens the conjugation of this double bond with the double bond in the neighbouring carboxyl group.

Activation of carbonyl group seems to depend on the properties of the oxide support. Namely, the more reducible and electrophilic the oxide support is, the more likely it is that mesityl oxide adsorption incorporates carbonyl group so that highly activated intermediate products presumably easily interacting with active hydrogen moieties are formed.

The overall observed catalytic reaction output may be different from what is suggested by favoured adsorbed intermediate products.[55] According to Loffreda and co-workers[56,57] some final products may not be obtained, at least not in large quantities, due to their desorption from the catalyst surface being the limiting step. Hindered desorption may, thus, allow achieving other compounds with good yields.

Mesityl oxide was chosen as the model compound due to being the simplest α,β-unsaturated ketone with similar steric hindrance around both C=C and C=O bonds, thus creating no bias on hydrogenation pathway. The choice of the organic compound and the catalyst determines hydrogenation product and reaction pathway. Hence, adsorption of prenal (3-methylbut-2-enal) on Pt (111) also involved formation of enol-type species,[55] but use of crotonaldehyde, furfural and cinnamaldehyde with NiBi intermetallic compound revealed adsorption of only C=O group, whilst 2 bands at 1650–1550 $cm^{-1}$ characteristic for "free state" C=C were observed at the same time.[8] Others suggest significant role of keto–enol tautomerisation in hydrogenation mechanism (studied on the example of acetophenone), as the tautomer can be stabilised by another molecule being the ketone.[58]

Our next step is to perform *in operando* PXRD studies focused on relating the crystal structure changes of the solid powder heterogeneous catalyst (all crystal phases) with its chemical activity. The research we have presented in this work is vital for understanding the catalytic properties of the selected systems to later interpret properly the crystal structure dynamics under *in operando* conditions. Some of the reaction conditions were deliberately not optimised because the PXRD system that we are commissioning after adopting it to work with vapours of liquids imposes slight limitations on how the chemical reaction can be carried out. The crucial condition is the reagents and products to be in the gas phase.

## Author contributions

MZ – conceptualisation, data curation, formal analysis, funding acquisition, investigation, methodology, project administration, resources, supervision, validation, visualisation, writing – original draft, writing – review & editing.

WJ – investigation, validation, resources, writing – review & editing.

ZK – formal analysis, funding acquisition, supervision, writing – review & editing.

## Conflicts of interest

There are no conflicts to declare.

## Acknowledgements

## References

1 J. Guzman and B. C. Gates, *Angew. Chem.*, 2003, **42**, 690.

2 X. Zhang, H. Shi and B. Xu, *Angew. Chem.*, 2005, **44**, 7132.

3 X. Zhang, F. X. LlabresiXamena and A. Corma, *J. Catal.*, 2009, **265**, 155.

4 X. Xue, M. Niu, Y. Xu and Y. Wang, *RSC Adv.*, 2017, 7, 50343.

5 D. Gizinski, I. Goszewska, M. Zielinski, D. Lisovytskiy, K. Nikiforov, J. Masternak, M. Zienkiewicz-Machnik and A. Srebowata, *Catal. Commun.*, 2017, **98**, 17.

6 L. Zeyang, W. Yongjie, L. Kaihong, W. Shanshan, L. Haocheng, Z. Yuanli, H. Baoming, T. Chunxia and L. Guohua, *Front. Chem.*, 2021, **9**, 781.

7 Y. Cao, J. Guerrero-Sańchez, I. Lee, X. Zhou, N. Takeuchi and F. Zaera, *ACS Catal.*, 2020, **10**, 3431.

8 J. Yu, Y. Yang, L. Chen, Z. Li, W. Liu, E. Xu, Y. Zhang, S. Hong, X. Zhang and M. Wei, *Appl. Catal., B*, 2020, **277**, 119273.

9 K. Wang and B. Yang, *Catal. Sci. Technol.*, 2017, **7**, 4024.

10 L. Kuai, Z. Chen, S. Liu, E. Kan, N. Yu, Y. Ren, C. Fang, X. Li, Y. Li and B. Geng, *Nat. Commun.*, 2020, **11**, 48.

11 X. Huang, T. Jones, A. Fedorov, R. Farra, C. Coperet, R. Schlogl and M.-G. Willinger, *Adv. Mater.*, 2021, **33**, 2101772.

12 Z. Kaszkur, P. Rzeszotarski and W. Juszczyk, *J. Appl. Crystallogr.*, 2014, **47**, 2069.

13 Z. Kaszkur, M. Zielinski and W. Juszczyk, *J. Appl. Crystallogr.*, 2017, **50**, 585.

14 A. J. Gellman, W. T. Tysoe and F. Zaera, *Catal. Lett.*, 2015, **145**, 220.

15 User manuals of printers manufactured by Brother (TM).

16 C. Wawrzenczyk and K. Wisinska, *Pol. J. Chem.*, 2007, **81**, 1887.

17 W. T. Tysoe and S. P. Roy, Enantioselective reduction of ketones on clean and chirally modified single crystal model Pd and Pt catalysts, in *Abstracts of Papers*, 262nd ACS National Meeting & Exposition, Atlanta, GA, United States, 2021.

18 R. Ciriminna, M. Pagliaro, E. Falletta, C. P. Della and J. H. Teles, *Angew. Chem., Int. Ed.*, 2016, **55**(46), 14210.

19 T. Ishida, H. Koga, M. Okumura and M. Haruta, *Chem. Rec.*, 2016, **16**, 2278.

20 X. Liu, M.-H. Liu, Y.-C. Luo, C.-Y. Mou, S. D. Lin, H. Cheng, J.-M. Chen, J.-F. Lee and T.-S. Lin, *J. Am. Chem. Soc.*, 2012, **134**(24), 10251.

21 M. A. Saqlain, A. Hussain, M. Siddiq and A. A. Leitao, *Appl. Catal., A*, 2016, **519**, 27.

22 Y.-G. Wang, D. C. Cantu, M.-S. Lee, J. Li, V.-A. Glezakou and R. Rousseau, *J. Am. Chem. Soc.*, 2016, **138**(33), 10467.

23 M. Haruta, *CATTECH*, 2002, **6**(3), 102.

24 M. Zielinski, Master thesis Warszawa, Warsaw University of Technology, Faculty of Chemistry, Poland, 2015, https://apd.usos.pw.edu.pl/diplomas/4922/.

25 Y. L. Lam and M. Boudart, *J. Catal.*, 1977, **50**, 530.

26 B. P. Block and J. C Bailar, *J. Am. Chem. Soc.*, 1951, **73**, 4722.

27 W. J. Louw and W. Robb, *Inorg. Chim. Acta*, 1969, **3**(1), 29.

28 K. Kitada, inventor, *US Pat.*, 6087516, 2000.

29 Merck KGaA, *Material Safety Data Sheet: Mesityl oxide for synthesis Darmstadt*, Germany, 2015.

30 Fisher Scientific – Acros Organics, *Material Safety Data Sheet: 4-methyl-2-pentanol Fair Lawn*, NJ, USA; 2018.

31 R. P. Young and N. Sheppard, *J. Catal.*, 1967, **7**, 223.

32 D. M. Griffiths and C. H. Rochester, *J. Chem. Soc., Faraday Trans.*, 1978, **74**, 403.

33 B. E. Hanson, L. F. Wieserman, G. W. Wagner and R. A. Kaufman, *Langmuir*, 1987, **3**(4), 549.

34 M. El-Mazawi, A. N. Finken, A. B. Nair and V. H. Grassian, *J. Catal.*, 2000, **191**, 138.

35 G. Busca and V. Lorenzelli, *J. Chem. Soc., Faraday Trans.*, 1982, **78**, 2911.

36 F. Braun and J. I. Di Cosimo, *Catal. Today*, 2006, **116**, 206.

37 A. Panov and J. J. Fripiat, *Langmuir*, 1998, **14**, 3788.

38 I. P. Silverwood, S. M. Rogers, S. K. Callear, S. F. Parker and C. R. A. Catlow, *Chem. Commun.*, 2016, **52**, 533.

39 W. L. Watkins and Y. Borensztein, *Phys. Chem. Chem. Phys.*, 2017, **19**, 27397.

40 F. Delbecq and P. Sautet, *J. Catal.*, 1995, **152**(2), 217.

41 X. Lan and T. Wang, *ACS Catal.*, 2020, **10**, 2764.

42 M. Zielinski, W. Juszczyk, J. W. Sobczak and Z. Kaszkur, *Phys. Chem. Chem. Phys.*, 2022, under review.

43 C. Binet, A. Badri, M. Boutonnet-Kizling and J.-C. Lavalley, *J. Chem. Soc., Faraday Trans.*, 1994, **90**, 1023.

44 D. G. Araiza, A. Gomez-Cortes and G. Diaz, *Catal. Sci. Technol.*, 2017, **7**, 5224.

45 C. Schilling, M. Ziemba, C. Hess and V. Ganduglia-Pirovano, *J. Catal.*, 2020, **383**, 264.

46 M. Morgensen, N. M. Sammes and G. A. Tompsett, *Solid State Ionics*, 2000, **129**, 63.

47 M. M. Khader, F. M. N. Kheiri, B. E. El-Anadouli and B. G. Ateya, *J. Phys. Chem.*, 1993, **97**, 6074.

48 J. L. Murray and H. A. Wriedt, *Bull. Alloy Phase Diagrams*, 1987, **8**(2), 148.

49 M. Zielinski, PhD Thesis, Institute of Physical Chemistry, Polish Academy of Sciences, Warszawa, Poland, 2019, https://rcin.org.pl/dlibra/publication/edition/81875?id=81875.

50 R. W. G. Wyckoff, *Crystal structures*, Interscience Publishers, New York, London, Sydney, 2nd edn, 1963.

51 H. Hofmeister, Fivefold Twinned Nanoarticles, *Encycl. Nanosci. Nanotechnol.*, 2003, **10**, 1–22.

52 A. S. Barnard, N. P. Young, A. I. Kirkland, M. A. van Huis and H. Xu, *ACS Nano*, 2009, **3**(6), 1431.

53 A. I. Kirkland, D. A. Jefferson, D. Tang and P. P. Edwards, *Proc. R. Soc. London, Ser. A*, 1991, **434**(1891), 279.

54 C. Ling and Y. Yu, *IUCrJ*, 2019, **6**, 447.

55 C. J. Kliewer, M. Bieri and G. A. Somorjai, *J. Am. Chem. Soc.*, 2009, **131**, 9958.

56 D. Loffreda, F. Delbecq, F. Vigne and P. Sautet, *J. Am. Chem. Soc.*, 2006, **128**(4), 1316.

57 D. Loffreda, F. Delbecq, F. Vigne and P. Sautet, *Angew. Chem., Int. Ed.*, 2005, **44**, 5279.

58 S. Attia, M. C. Schmidt, C. Schoeder, J. Weber, A.-K. Baumann and S. Schauermann, *J. Phys. Chem. C*, 2019, **123**(48), 29271.

59 M. von Laue, *Ann. Phys.*, 1926, **81**, 877.

60 A. G. Panov and J. J. Fripiat, *J. Catal.*, 1998, **178**, 188.

61 D. M. Griffiths and C. H. Rochester, *J. Chem. Soc., Faraday Trans.*, 1977, **73**, 1988.

62 H. Miyata, Y. Toda and Y. Kubokawa, *J. Catal.*, 1974, **32**, 155.

63 M. Bonarowska, M. Wojciechowska, M. Zielinski, A. Kiderys, M. Zielinski, P. Winiarek and Z. Karpinski, *Molecules*, 2016, **21**, 1620.

64 S. Benbenek, E. Fedorynska and P. Winiarek, *React. Kinet. Catal. Lett.*, 1993, **51**(1), 189.

65 P. Zielinska, *Master Thesis Warszawa*, Warsaw University of Technology, Faculty of Chemistry, Poland, 2015, https://repo.pw.edu.pl/info/master/WUT992802c1f859492bb1dbed999a309fae/.